ELSEVIER

Biomaterials 23 (2002) 4541–4547

Biomaterials

www.elsevier.com/locate/biomaterials

Transformation mechanism of different chemically precipitated apatitic precursors into β-tricalcium phosphate upon calcination

Sz-Chian Liou, San-Yuan Chen*

Department of Materials Science and Engineering, National Chiao-Tung University, 1001 Ta-hsueh Road, Hsinchu 300, Taiwan ROC

Received 16 January 2002; accepted 15 May 2002

Abstract

The Ca-deficient apatite (CDHA) was prepared from the precursors of $(CH_3COO)_2Ca \cdot xH_2O$, $Ca(NO_3)_2 \cdot 4H_2O$ and H_3PO_4, $(NH_4)H_2PO_4$ to investigate the transformation mechanism of β-tricalcium phosphate (β-TCP). X-ray diffraction analysis shows that the development of β-TCP is not via direct reaction between Ca and P for all the different combinations between Ca and P precursors. The activation energy of β-TCP formation with $(NH_4)H_2PO_4$ as precursor was higher than that with H_3PO_4. Following the Johnson–Mehl–Avrami equation, the reaction kinetics of β-TCP phase formation is found one-dimension growth with interface-controlled and diffusion controlled growth depending on the annealing temperature. There exists a transition between 750°C and 825°C, and the transition rate from interface-controlled to diffusion-controlled growth is precursor-dependent.

Keywords: Ca-deficient apatite; β-tricalcium phosphate; JMA equation; Transformation kinetics

1. Introduction

Bioactive ceramic materials, such as hydroxyapatite (HA) or tricalcium phosphate (TCP), were introduced as bone substitutes. Due to the chemical similarity between HA and mineralized bone of human tissue, synthetic HA exhibits strong affinity to host hard tissues [1]. TCP has been shown to be resorbable in vivo with new bone growth replacing the implanted TCP [2]. This property is a significant advantage of TCP compared to other biomedical materials that are not resorbable. Two techniques were usually adopted for the preparation of β-TCP. One is solid-state reaction [3–5] and the other is "wet-chemical method" [6–19]. The latter method was most commonly used but usually results in the formation of a non-stoichiometric apatite whose molar ratio of Ca/P is from 1.33 to 1.65 [6,7,10–14]. Non-stoichiometric apatite with formula $Ca_{10-x}(HPO_4)_x(PO4)_{6-x}(OH)_{2-x}$ $(0 \leqslant x \leqslant 1)$ exhibits the same crystal structure as stoichiometric HA. When Ca/P molar ratio is equal to 1.5, corresponding to $x = 1$ in the above-mentioned formula, the $Ca_9(HPO_4)(PO_4)_5(OH)$ is called Ca-deficient apatite (CDHA), which has an apatite crystal structure and the molar ratio of Ca/P is equal to TCP (Ca/P = 1.5). When the CDHA was calcined above 700–800°C, it will be transformed into β-TCP, as described by Eq. (1).

$$Ca_9(HPO_4)(PO_4)_5(OH) \rightarrow 3Ca_3(PO_4)_2 + H_2O. \quad (1)$$

The phase transformation from CDHA to β-TCP has been investigated by using X-ray diffraction (XRD) and FT-IR spectra [7,10–13,15,20–22]. However, very few papers have been focused on the transformation kinetics from CDHA to β-TCP although several studies have paid attention to the formation mechanism of HA [23–27]. Recently, Lopatin et al. studied the crystallization kinetics of sol–gel derived HA and TCP and reported that the activation energies for amorphous to HA and HA to TCP are 189 and 492 kJ/mol, and n values are 0.66 and 1.5 for both transformations, respectively [27]. However, no systematical discussion was made especially for the wet-chemical derived powder since the transformation kinetics as well as activation energy are sensitive to phase structure/composition of initially prepared materials. Therefore, different precursors will be used to study the phase evolution from CDHA to β-TCP in this work. The effect of precursors on the

*Corresponding author. Tel.: +886-3-573-1818; fax: +886-3-5725490.

E-mail address: sychen@cc.nctu.edu.tw (S.-Y. Chen).

0142-9612/02/$ - see front matter
PII: S0142-9612(02)00198-9

formation mechanism of β-TCP with annealing temperature is also proposed to clarify the role of precursor.

2. Experimental procedure

2.1. Sample preparation

The starting materials used in this investigation were analytical grade reagents $(CH_3COO)_2Ca \cdot xH_2O$ (99%, Aldrich Chemical company, Inc., USA) and $Ca(NO_3)_2 \cdot 4H_2O$ (99%, Alfa Aesar, USA) as the Ca sources, and H_3PO_4 (99%, Riedel-deHaen, Seelze, Germany) and $(NH_4)H_2PO_4$ (98%, Aldrich Chemical Company, Inc., USA) as the P sources. Four systems were prepared to yield the stoichiometric ratio of Ca/P = 1.5 and summarized in Table 1. Both H_3PO_4 and $(NH_4)H_2PO_4$ solutions were dissolved in deionized water and slowly dropped into the vigorously stirred $(CH_3COO)_2Ca \cdot xH_2O$ and $Ca(NO_3)_2 \cdot 4H_2O$ aqueous solution for 2 h at room temperature. The pH value for all of the solutions was adjusted above 9 with ammonia solution (Merck). After filtering and washing, the mixture was dried overnight at 120°C. The dried powder was placed in an Al_2O_3 crucible, heated at a desired temperature for various holding time, using a heating rate of 10°C/min, and then rapidly quenched in air. The quenched powder was ground for X-ray diffractometer analysis to determine the formed amount of β-TCP.

2.2. Phase analysis

X-ray diffractometer (M18XHF, Mac Science, Tokyo, Japan) was used for determining the phase structure and the degree of reaction. The scanning rate of $4°2\theta$ per min over a range of $2\theta = 20-60°$ was used for phase identification. For kinetic study, the scanning rate was $0.5°2\theta$ per min over a range of $2\theta = 28-33°$. Reaction kinetic data were accumulated by integrating the β-TCP (0 2 10) peak area for each sample. The fraction of β-TCP at any time t, was calculated by comparing the (0 2 10) peak area ($2\theta = 31.02°$) of the sample containing 100% β-TCP to that of the partially reached sample, i.e., fraction of fraction $f = A_t/A_{100\%\beta\text{-TCP}}$. Each datum appearing on the calcinations temperature/time curves was the average of three test results. The deviation of the data was around 5%.

For TEM analysis, the powder sample was ultrasonically dispersed in ethanol to form very dilute suspensions and then a few droplets were dropped on copper grids with carbon coated. Transmission electron microscopy (TEM, JEOL-2000FX), operating at an accelerating voltage of 200 kV, was used to observe the powder morphology. Fourier transform Infrared ray (FT-IR) spectra were performed using KBr pellets (2 mg per 300 mg KBr) on a spectrometer (Model 580, Perkin–Elmer) with a resolution of 4.00 cm^{-1}. Infrared spectra were recorded in the range of 4000–400 cm^{-1} to evaluate the function group of the specimens.

Table 1
Molar concentrations and pH values of the four solutions

System	A	B	C	D
$(CH_3COO)_2 \cdot Ca \cdot xH_2O$	0.15 M	0.15 M		
$Ca(NO_3)_2 \cdot 4H_2O$			0.15 M	0.15 M
H_3PO_4	0.1 M		0.1 M	
$NH_4H_2PO_4$		0.1 M		0.1 M
Initial pH	10	10	10	10
Final pH	10	10	10	10

3. Results and discussion

3.1. Crystalline phases

The XRD patterns for the four aqueous systems dried overnight at 120°C are shown in Fig. 1. Similar XRD patterns are obtained for these systems and can be indexed as CDHA phase according to ICDD No. 9-432. The needle-like particles can be observed by transmission electron microscopy as shown in Fig. 2, and are rather similar to that of stoichiometric HA or non-stoichiometric apatite synthesized by wet-chemical processing [28–40]. An axial zone in some needle-like particles can be clearly observed as marked with the arrows in Fig. 2. Suvorova et al. reported that the needle-like HA easily forms aggregated crystal when higher concentration and fast mixing were applied to the solutions [35]. Mao et al. suggested that the HA crystals tend to grow along [0 0 0 1] direction, the fastest growth direction, resulting in needle-like morphology [36].

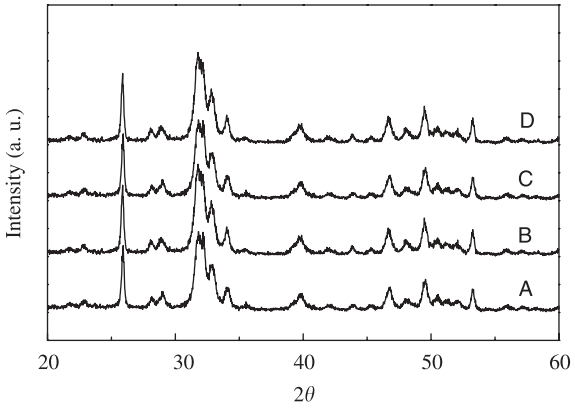

Fig. 1. XRD patterns of as-prepared samples for four aqueous systems.

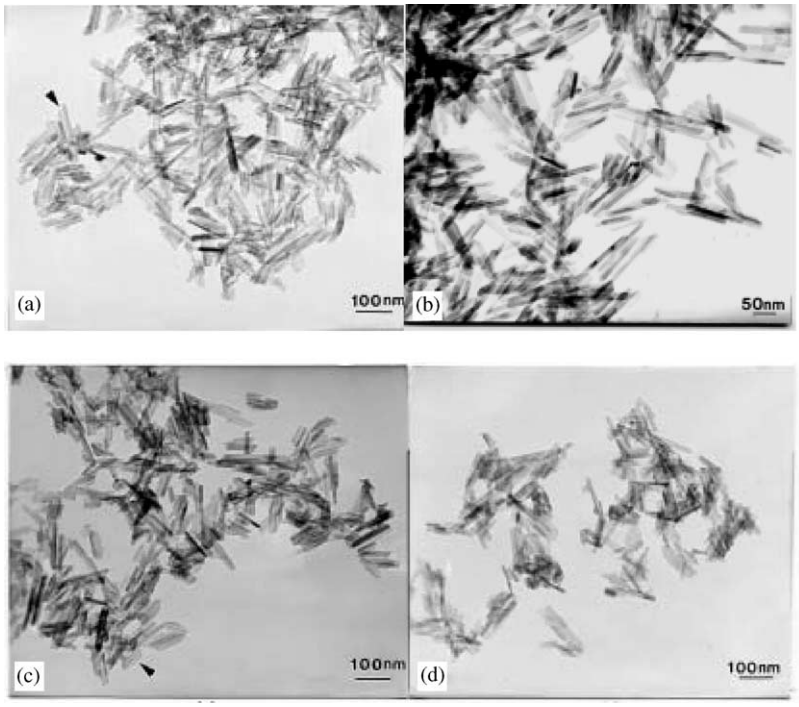

Fig. 2. TEM bright field (BF) image of as-prepared samples for (a) system A, (b) system B, (c) system C and (d) system D.

Fig. 3 illustrates the FT-IR absorption spectra of the as-prepared samples. The bands at 1092 and 1040 cm^{-1} are assigned to the components of the triply degenerate v_3 antisymmetric P–O stretching mode. The 962 cm^{-1} band is assigned to v_1, the non-degenerate P–O symmetric stretching mode. The bands at 601 and 571 cm^{-1} are assigned to components of the triply degenerate v_4 O–P–O bending mode and the bands in the range of 462–474 cm^{-1} are assigned to the components of the doubly degenerate v_2 O–P–O bending mode. Molecular and adsorbed water bands are also discerned at 1640 and 3400 cm^{-1}. A significant concentration of hydroxyl groups remains in the structure as observed from the intensity of the stretching and librational bands at 3572 and 632 cm^{-1} [41–45]. In addition, the band at 1380–1403 cm^{-1} assigned to NH_4^+ was only observed in systems B and D [46]. This phenomenon is possibly related to the fact that different P precursors, H_3PO_4 and $(NH_4)H_2PO_4$, were used in our study. A very weak band near 875 cm^{-1} is possible the P–O(H) stretching in HPO_4^{2-} groups or v_2 vibration mode of CO_3^{2-} groups. However, no v_3 vibration mode (near 1490 and 1426 cm^{-1}) of CO_3^{2-} groups was observed in the FT-IR spectra. Therefore, it was believed that the weak peak at 875 cm^{-1} was primarily characteristic of the HPO_4^{2-} although CO_2 has a very affinity to apatite crystal during the synthesis process.

The phase transformation from CDHA to β-TCP was performed by heating the samples at the temperature range of 500–1000°C with a heating rate of 10°C/min.

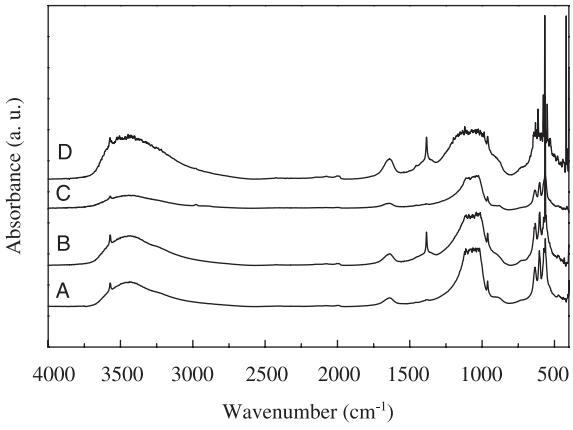

Fig. 3. FT-IR spectra of as-prepared samples for (A) system A, (B) system B, (C) system C, and (D) system D.

After the required temperature was reached, it was immediately cooled to room temperature without maintaining any time in this indicated temperature. Fig. 4 shows that the phase transformation in system A occurs within the temperature region of 800–900°C. In order to close inspect the transformation, similar experiments were performed for system A at 10°C intervals between 800°C and 900°C (without any holding). Fig. 5 reveals that within this temperature range, a two-phase mixture of CDHA and β-TCP, according to ICDD No. 9-169, was obtained. A small mount β-TCP occurred at 810°C and CDHA

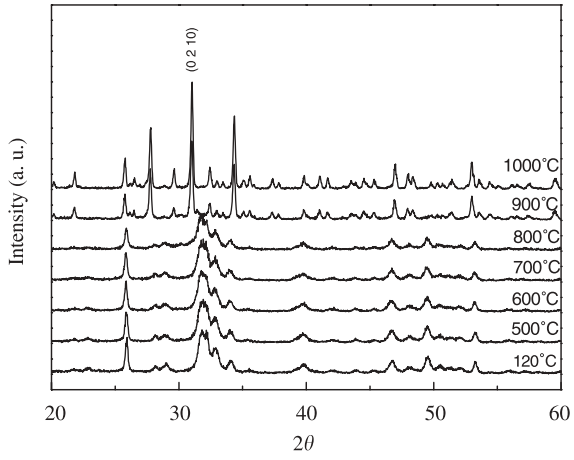

Fig. 4. XRD patterns of system A annealed at different temperatures.

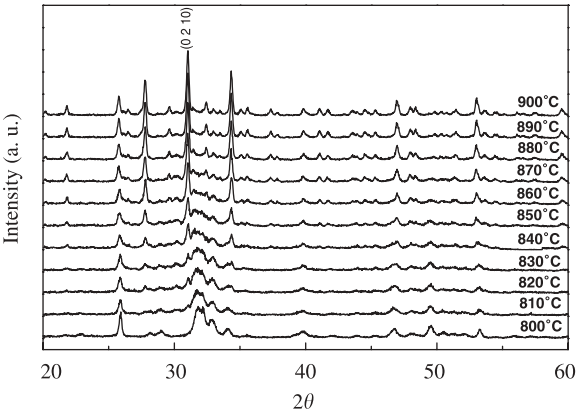

Fig. 5. XRD patterns of system A showing the transformation from CDHA to β-TCP crystalline over a narrow temperature range of between 810°C and 900°C.

disappeared above 900°C. Similar phase transformation of CDHA to β-TCP was observed in the other three aqueous systems. It seems to imply that the final product was not affected by the starting Ca and P precursors upon acid-base reaction. Similar phenomenon is also reported in other wet chemical methods [7,10–13]. However, it was noted that the pH value of the solution during the synthesis has a decisive effect on the dissociation of the H_3PO_4 and $NH_4H_2PO_4$ reagent, the characteristic of precipitates and further phase reaction [11]. That is because in both H_3PO_4 and $NH_4H_2PO_4$ solutions, the PO_4^{3-} ions start to dominate only above a critical pH value. At a lower pH value, a large number of protonated phosphate ions, i.e., $H_2PO_4^{1-}$ and HPO_4^{2-}, are present in the solution. On the other hand, the increase in solution pH promotes the dissociation of H_3PO_4 and $NH_4H_2PO_4$ and enhances the formation of PO_4^{3-}.

3.2. Reaction kinetic

XRD traces from the four aqueous systems heated at 700–825°C for different periods were taken to investigate the reaction kinetics. Fig. 6 shows the phase evolution of system A isothermally annealed at 700°C. It was observed that the minute β-TCP starts to appear in 1 h and completely forms at 30 h. The formation fraction of β-TCP in the system A fired at 700–825°C as a function of time was shown in Fig. 7. All of the transformation curves are sigmoidal in shape, indicating that the formation of β-TCP proceeds with nucleation and growth processes. The crystallization rate, as characterized by the slopes in the rapidly rising portion, increases with the increase of annealing temperature. A solid-state reaction model derived by Johnson–Mehl–Avrami (JMA) equation was used to investigate the reaction kinetics of β-TCP formation [47–49].

$$f = 1 - \exp(-kt^n), \tag{3}$$

where f is the formed fraction of β-TCP at time t, k rate constant, and n the Avrami exponent. The possible n

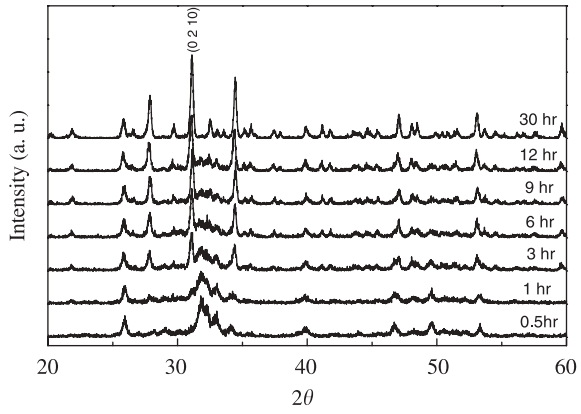

Fig. 6. XRD patterns of system A isothermally annealed at 700°C for different times in air.

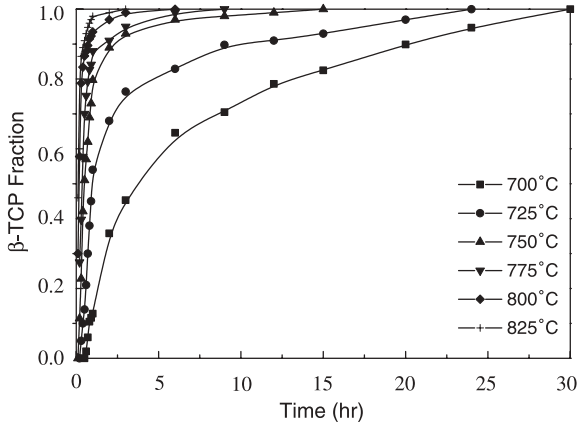

Fig. 7. Transformed β-TCP amount of system A fired at 700–825°C for different times in air.

values, depending on the mechanism of phase transformation, are listed in Table 2 [50]. Both values of n and k can be calculated by rearranging Eq. (3) as follows:

$$\ln\{\ln[1/(1-f)]\} = \ln k + n \ln t. \quad (4)$$

The data shown in Fig. 7 can be replotted as $\ln\{\ln[1/(1-f)]\}$ vs. $\ln t$ and given in Fig. 8. Using the linear least-squares fit method, both values of n and $\ln k$ can be calculated from the slopes and the intercepts of these lines. Following the Arrhenius relationship ($\ln k$ vs. $1/T$), the activation energy of β-TCP formation from 700°C to 750°C can be calculated as ~261.4, 336.2, 264.9 and 352.7 kJ/mol for systems A, B, C and D, respectively. When NH_4^+ ions were adsorbed on the surface of the powders, it leads to the reduction of the phase transformation reaction. Therefore, a higher energy was required for the transformation of CDHA into β-TCP in both systems B and D than both systems A and C due to the absorption of NH_4^+ on the powder surface. If they adsorbed only to powder surface, two situations might happen: physical and chemical adsorption. However, from the previous study, it should be a sort of chemical adsorption. If it does, then they are strongly bonded to the lattice defect and make a further transformation of lattice structure more difficult, so does the energy term [51]. As shown in Fig. 9, the n values of the four systems vary with annealing temperatures. It seems to indicate that there exist different transformation mechanisms from CDHA to β-TCP between low temperature (700°C) and high temperature (825°C). Since the particle of β-TCP phase presents lath-shaped morphology, shown in Fig. 10, it might suggest that the reaction belongs to one-dimension growth. When all of the systems were annealed between 700°C and 750°C, a nearly constant n value of 0.95 was obtained, which reflects that the reaction is probably an interface-controlled growth.

When the samples were heated above 750°C, it was found that the n values decrease with increasing temperature. Furthermore, systems A and C exhibit similar behavior but show different trend as comparing with that of systems B and D. In other words, during the

Table 2
Theoretical values of Avrami exponent, n [50]

		Interface-controlled growth	Diffusion-controlled growth
3D	Constant nucleation rate	$n = 4$	$n = 2.5$
	Instantaneous nucleation	$n = 3$	$n = 1.5$
	Decreasing nucleation rate	$n = 3-4$	$n = 1.5-2.5$
2D	Constant nucleation rate	$n = 3$	$n = 2$
	Instantaneous nucleation	$n = 2$	$n = 1$
	Decreasing nucleation rate	$n = 2-3$	$n = 1-2$
1D	Constant nucleation rate	$n = 2$	$n = 1.5$
	Instantaneous nucleation	$n = 1$	$n = 0.5$
	Decreasing nucleation rate	$n = 1-2$	$n = 0.5-1.5$

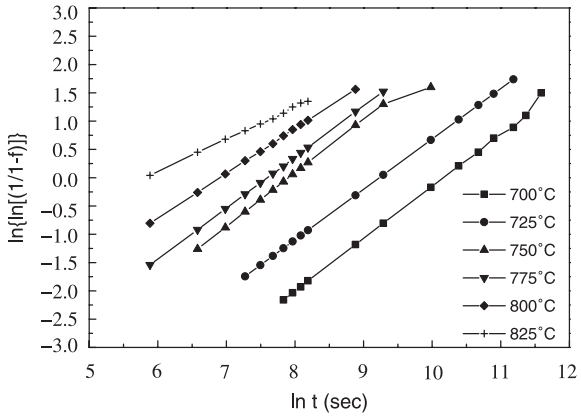

Fig. 8. Avrami's analysis according to Eq. (4) to determine n and k of system A at different temperatures.

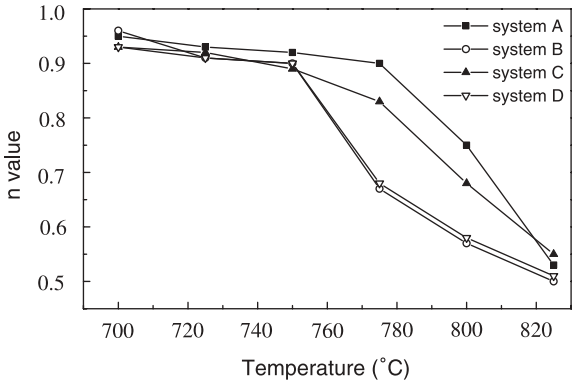

Fig. 9. The n values dependence of isothermal annealing temperatures for the four systems.

Fig. 10. TEM bright field (BF) image of system A annealed at 700°C for 2 h.

transition stage between 750°C and 825°C, the decrease of n value with increasing temperature is faster in the latter (systems B and D) than the former (systems A and C). Lopatin et al. studied both transformations of amorphous to HA and HA to TCP and reported that the n values are 0.66 and 1.5 for the former and the latter, respectively [27]. It was reported that the difference in n values are dependent on the composition change between the two phases from $[Ca/P]_{HA} = 1.667$ to $[Ca/P]_{TCP} = 1.5$. However, in our case, the Ca/P ratio in all the studied systems is constant (1.5).

Therefore, it is believed that the different behavior between these two types is found strongly dependent on the starting phosphate precursors. In systems A and C, H_3PO_4 was used as the P precursor. On the other hand, systems B and D employed the $(NH_4)H_2PO_4$ as the P precursor. As the annealing temperature exceeds 825°C, the n values become close to 0.5, indicating that the reaction ($n = 0.5$) is dominated by diffusion-controlled growth.

4. Conclusions

(1) The phase evolution from CDHA to β-TCP occurs independent of Ca and P precursors.
(2) The activation energy of β-TCP phase formation with $(NH_4)H_2PO_4$ as the precursor was higher than that with H_3PO_4.
(3) The reaction kinetics of β-TCP phase formation is found one-dimension growth with interface-controlled at temperature below 750°C but becomes diffusion-controlled at the annealing temperature more than 825°C.
(4) There exists a transition from interface-controlled to diffusion-controlled growth and transition rate is precursor-dependent.

Acknowledgements

The authors would like to thank Dr. D.M. Liu for helpful discussion The authors gratefully acknowledge the National Science Council of the Republic of China for its financial support through Contract No. NSC-89-2216-E-009-034.

References

[1] Liu DM, Troczynski T, Tseng WJ. Water-based sol–gel synthesis of hydroxyapatite: process development. Biomaterials 2001;22:1721–30.
[2] Gatti AM, Zaffe D, Poli GP. Behavior of tricalcium phosphate and hydroxyapatite granules in sheep bone defects. Biomaterials 1990;11:513.
[3] TenHuisen KS, Brown PB. Phase evolution during the formation of β-tricalcium phosphate. J Am Ceram Soc 1999;82(10):2813–8.
[4] Yokogawa Y, Kawamoto Y, Toriyama M, Suzuki T, Kawamura S. Tricalcium phosphate coating on zirconia using calcium metaphosphate and tetracalcium phosphate. J Ceram Soc Japan 1991;99:28–31.
[5] Famery R, Richard N, Boch P. Preparation of α- and β-tricalcium phosphate ceramics, with and without magnesium addition. Ceram Int 1994;20:327–36.
[6] Jarcho M, Salsbury RL, Thomas MB, Doremus RH. Synthesis and fabrication of β-tricalcium phosphate (whitlockite) ceramics for potential prosthetic applications. J Mater Sci 1979;14:142–50.
[7] Akao M, Aoki H, Kato K, Sato A. Dence polycrystalline β-tricalcium phosphate for prosthetic applications. J Mater Sci 1982;17:343–6.
[8] Mortier A, Lemaitre J, Rodrique L, Rouxhet PG. Synthesis and thermal behavior of well-crystallized calcium-deficient phosphate apatite. J Solid State Chem 1989;78:215–9.
[9] Itatani K, Nishioka T, Seike S, Howell FS, Kishioka A, Kinoshita M. Sinterability of β-calcium orthophosphate powder prepared by spray-pyrolysis. J Am Ceram Soc 1994;77(3):801–5.
[10] Yubao L, Klein CPAT, Xingdong Z, de Groot K. Formation of a bone apatite-like layer on the surface of porous hydroxyapatite ceramics. Biomaterials 1994;15:835–41.
[11] Slosarczyk A, Stobierska E, Paszkiewicz Z, Gawlicki M. Calcium phosphate materials prepared from precipitates with various calcium phosphorus molar ratios. J Am Ceram Soc 1996;79(10):2539–44.
[12] Narasaraju TSB, Phebe DE. Review some physico-chemical aspects of hydroxylapatite. J Mater Sci 1996;31:1–21.
[13] Tas AC, Korkusus F, Timucin M, Akkas N. An investigation of the chemical synthesis and high-temperature sintering behavior of calcium hydroxyapatite (HA) and tricalcium phosphate (TCP) bioceramics. J Mater Sci Mater Med 1997;8:91–6.
[14] Vallet-Regi M, Rodriguez-Lorenzo LM, Salinas AJ. Synthesis and characterization of calcium deficient apatite. Solid State Ionic 1997;101–103:1279–85.
[15] Kivrak N, Tas AC. Synthesis of calcium hydroxyapatite-tricalcium phosphate (HA-TCP) composite bioceramic powders and their sintering behavior. J Am Ceram Soc 1998;81(9):2245–52.
[16] Tas AC. Combination synthesis of calcium phosphate bioceramics powders. J Europ Ceram Soc 2000;20:2389–94.
[17] Engin NO, Tas AC. Preparation of porous Ca_{10} $(PO_4)6(OH)_2$ and β-$Ca_3(PO_4)_2$ bioceramics. J Am Ceram Soc 2000;83(7):1581–4.
[18] Gibson IR, Rehman I, Best SM, Bonfield W. Characterization of the transformation from calcium-deficient apatite to β-tricalcium phosphate. J Mater Sci: Mater Med 2000;11:533–9.
[19] Arends J, Christoffersen J, Christoffersen MR, Eckert H, Fowler BO, Heughebaert JC, Nancollas GH, Yesinowski JP, Zawacki SJ. A calcium hydroxyapatite precipitated from an aqueous solution: an international multimethod analysis. J Cryst Growth 1987;84:515–32.
[20] Hata K, Kokubo T, Nakamura T, Yamamuro T. Growth of a bonelike layer on a substrate by a biomimitic process. J Am Ceram Soc 1995;78(4):1049–53.
[21] Ishikawa K, Ducheyne P, Radin S. Determination of the Ca/P ratio in calcium-deficient hydroxyapatite using X-ray diffraction analysis. J Mater Sci: Mater in Medicine 1993;4:165–8.
[22] Smiciklas ID, Milonjic SK, Zec S. An inverse gas chromatographic study of the adsorption of alkanes on hydroxyapatite. J Mater Sci 2000;35:2825–8.

[23] Brown PW, Fulmer M. Kinetics of hydroxyapatite formation at low temperature. J Am Ceram Soc 1991;74(5):934–40.
[24] Brown PW, Hocker N, Hoyle S. Variations in solution chemistry during the low temperature formation of hydroxyapatite. J Am Ceram Soc 1991;74(8):1848–54.
[25] Cihlar J, Buchal A, Trunec M. Kinetics of thermal decomposition of hydroxyapatite bioceramics. J Mater Sci 1999;34:6121–31.
[26] Liu C, Huang Y, Shen W, Cui J. Kinetics of hydroxyapatite precipitation at pH 10 to 11. Biomaterials 2001;22:301–6.
[27] Lopatin CM, Pizziconi VB, Alford TL. Crystallization kinetics of sol–gel derived hydroxyapatite thin films. J Mater Sci: Mater Med 2001;12:767–73.
[28] Puech J, Heughebaert JC, Montel G. A new mode of growing apatite crystallites. J Cryst Growth 1982;56:20–4.
[29] Ji H, Marquis PM. Preparation and characterization of Al_2O_3 reinforced hrdroxyapatite. Biomaterials 1992;13(11):744–8.
[30] Yubao L, Klein CPAT, De Wijn J, Van De Meer S, De Groot K. Shape change and phase transition of needle-like non-stoichiometric apatite crystals. J Mater Sci: Mater Med 1994;5:263–8.
[31] Yubao L, De Groot K, De Wijn J, Klein CPAT, Van De Meer S. Morphology and composition of nanograde calcium phosphate needle-like crystals formed by simple hydrothermal treatment. J Mater Sci: Mater Med 1994;5:326–31.
[32] Lu HB, Ma CL, Cui H, Zhou LF, Wang RZ, Cui FZ. Controlled crystallization of calcium phosphate under stearic acid monolayers. J Cryst Growth 1995;155:120–5.
[33] Madsen HEL, Christensson F, Polyak LE, Suvorova EI, Kliya MO, Chernov AA. Calcium phosphate crystallization under terrestrial and microgravity conditions. J Cryst Growth 1995;152:191–202.
[34] Suzuki S, Ohgaki M, Ichiyanagi M, Ozawa M. Preparation of needle-like hydroxyapatite. J Mater Sci Lett 1998;17:381–3.
[35] Suvorova EI, Christensson F, Madsen HEL, Chernov AA. Terrestrial and space-grown HAP and OCP crystals: effect of growth conditions on perfection and morphology. J Cryst Growth 1998;186:262–74.
[36] Mao C, Li H, Cui F, Ma C, Feng Q. Oriented growth of phosphates on polycrystalline titanium in a process mimicking biomineralization. J Cryst Growth 1999;206:308–21.
[37] Suvorova EI, Buffat PA. Electron diffraction from micro-and nanoparticles of hydroxyapatite. J Microscopy 1999;196:46–58.
[38] Rodriguez-Lorenzo LM, Vallet-Regi M. Controlled crystallization of calcium phosphate apatite. Chem Mater 2000;12:2460–5.
[39] Knowles JC, Calluct S, Georgiou G. Characterisation of the rheological properties and zeta potential of a range of hydroxyapatite powders. Biomaterials 2000;21:1387–92.
[40] Koumoulidis GC, Vaimakis TC, Sdoukos AT, Boukos NK, Trapalis CC. Preparation of hydroxyapatite lathlike particles using high-speed dispersing equipment. J Am Ceram Soc 2001;84(6):1203–8.
[41] Blakeslee KC, Condrate RA. Vibration spectra of hydrothermally prepared hydroxyapatites. J Am Ceram Soc 1971;54:559–63.
[42] Fowler BO. Infrared studies of apatite. I. Vibrational assignments for calcium, strontium, and barium hydroxyapatites utilizing isotopic substitution. Inorg Chem 1974;13(1):194–207.
[43] Yamashita K, Kanazawa T. Hydroxyapatite. Inorg Phosphate Mater, Mater Sci Monograph 1989;52:30.
[44] Slosarczky A, Paluszkiewicz C, Gawlicki M, Paszkiewicz Z. The FTIR spectroscopy and QXRD studies of calcium phosphate bases materials produced from the powder precursors with different Ca/P ratios. Ceram Intern 1997;23:297–304.
[45] Cheng ZH, Yasukawa A, Kandori K, Ishikawa T. FT-IR study on incorporation of CO_2 into calcium hydroxyapatite. J Chem Soc Faraday Trans 1998;94:1501–5.
[46] Nakamoto K. Infrared, Raman spectra of inorganic and coordination compounds. New York: Wiley, Part A:191.
[47] Avrami M. Kinetics of phase change: I. General theory. J Chem Phys 1939;7(12):1103–12.
[48] Avrami M. Kinetics of phase change: II. Transformation-time relations for random distribution of nuclei. J Chem Phys 1940;8(2):212–24.
[49] Avrami M. Kinetics of phase change: III. Granulation, phase change and microstructure. J Chem Phys 1941;9(12):177–84.
[50] Hulbert SF. Models for solid-state reactions in powdered compacts: a review. J Br Ceram Soc 1969;6(1):11–20.
[51] Meyer JL, Flower BO. Lattice defects in nonstoichiometric calcium hydroxyapatites. A chemical approach. Inorg Chem 1982;21:3029–35.